Deciphering the astrophotochemical inertness of H_3^+ at molecular level

Josene M. Toldo,[a,b,c] Jakob Staab,[a,d] Eduard Matito,[e,f] Cina Foroutan-Nejad,[g] and Henrik Ottosson[a]*

[a] *Department of Chemistry - Ångström, Uppsala University, Uppsala, Sweden;*

[b] *Aix-Marseille University, CNRS, ICR, Marseille, France;*

[c] *Université Claude Bernard Lyon 1, ENS de Lyon, CNRS, LCH, UMR 5182, Lyon, France;*

[d] *Department of Chemistry, The University of Manchester, Oxford Road, Manchester, UK;*

[e] *Donostia International Physics Center (DIPC), 20018 Donostia, Euskadi, Spain;*

[f] *Ikerbasque, Basque Foundation for Science, 48009 Bilbao, Euskadi, Spain;*

[g] *Institute of Organic Chemistry, Polish Academy of Sciences, Warsaw, Poland.*

Abstract: The trihydrogen cation, H_3^+, is unique in the Universe. It serves as the primary proton reservoir, driving essential astrochemical reactions, and it functions as a thermostat for giant gas planets. H_3^+ has also remarkably low photodissociation rate, explained by its exceptionally high first electronic excitation energy (19.3 eV). Herein we reveal the key factors behind this high energy: (*i*) aromatic stabilization in its electronic ground state, (*ii*) antiaromatic destabilization in its first excited state, and (*iii*) a high nuclear-to-electronic charge ratio (+3 *vs.* -2). Through comparisons with analogous π-conjugated carbocations, we find that ground state aromatic stabilization plus excited state antiaromatic destabilization raise the excitation energy of H_3^+ by 4.8 - 6.0 eV. Only with this increase can it fulfil its unique functions in space.

Triangular H_3^+ is the most abundant polyatomic ion in the interstellar medium, where it functions as the primary interstellar acid, initiating reactions that lead to more complex molecules (Figure 1A).(*1*-*3*) It further acts as a thermostat (coolant) in the upper atmospheres of giant gas planets,(*4*) and it has been postulated that it even could have functioned as a coolant in the primordial gas (though with a different mechanism than in the giant gas planets).(*5*) With three H atoms, it is the smallest molecule that exhibits aromaticity (σ-aromaticity),(*6*-*9*) a stabilizing molecular property.(*10*)

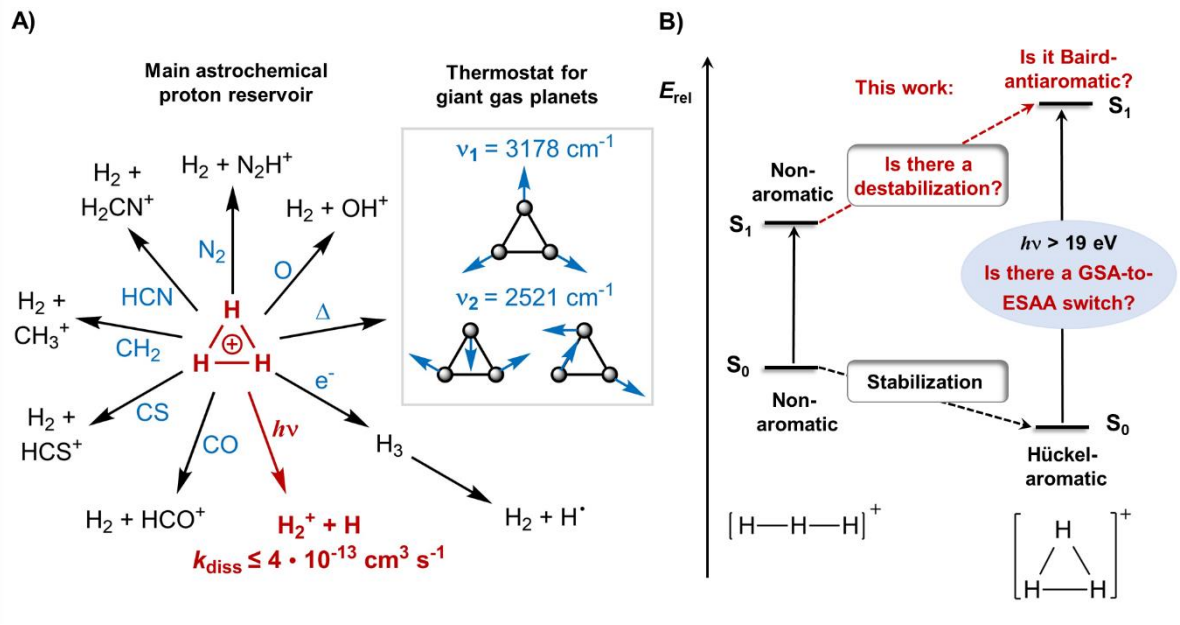

Figure 1: **The functions of H_3^+ in space and our working hypothesis on the origin of its very high excitation energy**: (A) A summary of the functions of H_3^+ in space, with its role as (*i*) primary proton reservoir initiating a number of core astrochemical reactions (typical rate constants for these are ~10^{-9} cm^3 s^{-1}), and (*ii*) as a thermostat in the upper atmospheres of giant gas planets ensuring that their temperatures do not exceed a threshold. (B) Tentative changes from the nonaromatic character of linear H_3^+ in its S_0 and S_1 states to the equilateral triangular H_3^+ with a stabilizing Hückel-aromaticity in S_0 (GSA = ground state aromaticity) and a destabilizing Baird-antiaromaticity in S_1 (ESAA = excited state antiaromaticity). Factors related to our hypothesis and explored herein written in red, while known factors in black.

The first vertically excited states of H_3^+, the doubly degenerate $1^1E'$ at the equilateral triangular structure (D_{3h} symmetric), are of exceptionally high energy (19.3 eV)(*11*) and they are dipole-allowed and dissociative.(*12-14*) Yet, despite this, astrochemical databases list a photodissociation rate of 4×10^{-13} s^{-1} or lower,(*13, 15*) whereby it is among the species with lowest photodissociation rates.(*16, 17*) The reason is that the much more abundant H and H_2, with ionization and excitation energies at 13.1 – 15.4 eV,(*1, 18*) shield H_3^+ from high-energy irradiation in the interstellar medium (ISM).(*12, 13, 19, 20*) In the ISM, H_3^+ degrades unimolecularly only when exposed to electrons ejected from other molecules or atoms upon cosmic ray ionization.(*1, 13*) Indeed, direct photodissociation only occurs when H_3^+ is rovibrationally excited, whereby the electronic excitation energy decreases down to 4.9 eV.(*12, 13*) Had it been more prone to photodissociate, this would have impaired its astrochemical and astrophysical functions, and thus, been detrimental to the development of the Universe. However, the molecular origins of its very high vertical excitation energy are unknown and have not been addressed earlier.

H_3^+ in S_0 has a D_{3h} symmetric structure (*11, 21-23*) with σ-aromatic character,(*6-9*) in line with Hückel's $4n+2$ rule (n = 0, 1, 2…) as it has two σ-electrons. We now argue that the concept of antiaromaticity (*10*) is crucial for the relative destabilization of its first excited states (Figure 1B), and thus its excitation energy. In this context, the analogous cyclic and fully π-conjugated hydrocarbons (*i.e.*, annulenes) in their lowest excited triplet states of ππ* character (T_1) follow Baird's rule.(*24-28*) This rule tells that molecules with $4n+2$ π-electrons are antiaromatic and destabilized in these states while those with $4n$ are aromatic and stabilized. Although derived for the T_1 state, the rule can often be extended to the lowest ππ* excited state of singlet multiplicity (S_1). Here we hypothesize that the exceptionally high excitation energy of H_3^+ stems from such σ-antiaromatic destabilization in S_1 (Figure 1B) combined with σ-

aromatic stabilization in S_0, *i.e.*, a switch in character from ground state Hückel-aromaticity (GSA) to excited state Baird-antiaromaticity (ESAA), a GSA-to-ESAA switch (Figure 1B). Herein, we investigated if the lowest excited states of H_3^+ are antiaromatic through quantum chemical calculations of various (anti)aromaticity descriptors, and what impact that has on the excitation energy. Computations were run at the EOM-CCSD level for all species, which for H_3^+ corresponds to a full configuration interaction (FCI) calculation, *i.e.*, a numerically exact solution of the Schrödinger equation. For further computational details, see SI section S1.

Potential energy surfaces

According to our computations, the H–H distances of equilateral triangular H_3^+ in S_0 are 0.875 Å (reference computed value: 0.873 Å (*11*)). The degenerate $1^1E'$ states appear vertically 19.28 eV above the S_0 state (Figure 2A and section S2), and the transition is symmetry allowed (f = 0.562). In C_{2v} symmetry, the $1^1E'$ states split into the 2^1A_1 and 1^1B_2 states (Figure 2B), where 2^1A_1 as S_1 dissociates to H_2^+ + H while 1^1B_2 as S_1 leads to 2 H(1s) + H^+.(*14*) The first triplet states (the degenerate $1^3E'$) have vertical excitation energies of 14.87 eV (Table 1) and exhibit similar dissociative behaviors as $1^1E'$. Lastly, the higher energy $1^1A_2''$ state in D_{3h} symmetry is a dissociative second-order saddle point with H–H distances of 1.620 Å. As this state involves an excitation from an a_1' orbital to a nonbonding Rydberg-type orbital a_2'' (Figure 2A), only one electron remains in a bonding molecular orbital (MO), which cannot counterbalance the electrostatic repulsion between three protons. For further results and discussions on this state, see Supplementary Information, sections S2 and S3.

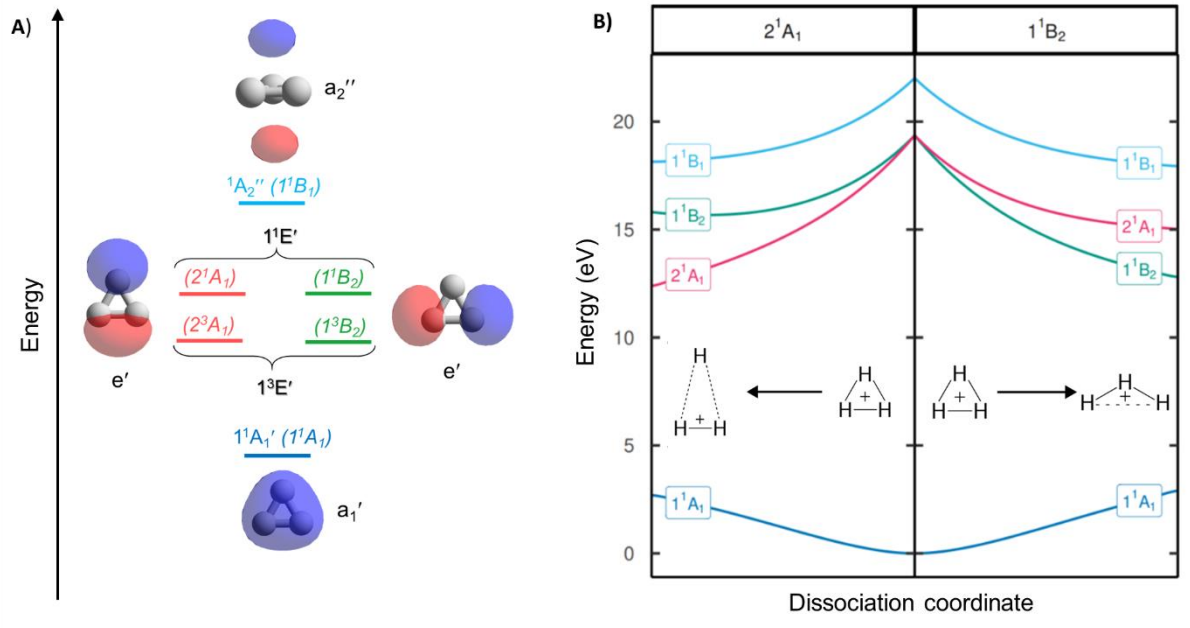

Figure 2. **Orbitals, electronic states, and potential energy surface profiles of H_3^+**: (A) The three valence MOs (a_1' and e'), the Rydberg orbital a_2'', and the labels of the electronic states within the D_{3h} (normal print) and C_{2v} (in parenthesis and italics) point groups. (B) Potential energy surface profiles of H_3^+ from the D_{3h} symmetric S_0 equilibrium geometry along the minimum energy path of the 2^1A_1 state keeping C_{2v} symmetry to an acute isosceles triangle (left), and along the minimum energy path of the 1^1B_2 state to an obtuse isosceles triangle (right).

Probing excited state antiaromaticity

The aromatic or antiaromatic characters of the various electronic states were determined by energetic, electronic, and magnetic (anti)aromaticity descriptors (for details see SI section S3 or reference (*10*)). To measure electron delocalization,(*29*) we use the two-center delocalization index (DI)(*30, 31*) and the normalized multicenter index ($MCI^{1/n}$)(*32*) that reflect the aromatic character. The magnetic response properties are explored by magnetically induced current densities (MICDs), and also by nucleus independent chemical shifts (NICSs). For details on the aromaticity descriptors, see Supplementary Information sections S3 and S4.

Although assessed earlier,(*6-9*) the values for σ-aromaticity of the S_0 state are discussed briefly in order to contrast the antiaromatic character of the excited states (*vide infra*). H_3^+ has two electrons and forms a 3-center 2-electron (3c-2e) bond both in its linear and triangular structures. Therefore, the energy gain when going from the linear to the triangular structure (1.76 eV) represents the extra cyclic resonance energy,(*33, 34*) reflecting an aromatic stabilization of cyclic H_3^+ in S_0 (Figure 1). The topological analysis also reveals a species that benefits from extensive 3c-2e bonding, manifested in the formation of a non-nuclear attractor (NNA) in the center (Figure 3A), in agreement with previous works.(*7, 8*) Large DI values between the hydrogen atoms and the large positive $MCI^{1/n}$ of 0.62 (Figure 3A)(*35*) are also consistent with σ-aromaticity in S_0 (the $MCI^{1/n}$ of benzene in S_0 is 0.59 (*36*)). Finally, H_3^+ in its S_0 state displays a diatropic MICD of 4.39 nA/T, in agreement with the $NICS(0)_{zz}$ value of -37.1 ppm, confirming the magnetic aromaticity of H_3^+ in S_0.

Evaluation of the potential antiaromaticity in the $1^1E'$ states of D_{3h} symmetric H_3^+ is more challenging, requiring separate characterizations of the two states, the 2^1A_1 and 1^1B_2 states in C_{2v} symmetry. Going from the linear ($D_{\infty h}$) to the triangular S_0 state equilibrium geometry of H_3^+ results in a destabilization in the lowest vertically excited singlet states by 4.19 eV (Figure 3B). This reveals a negative extra cyclic resonance energy indicating antiaromaticity. Thus, the stabilization in S_0 plus destabilization in $1^1E'$ upon cyclization have implications for the vertical excitation energy as this sum is 5.95 eV (Figure 3B). The corresponding sum for the lowest triplet states is 7.50 eV. Both energies are in line with GSA-to-ESAA switches in character upon vertical excitation (Figure 1B).

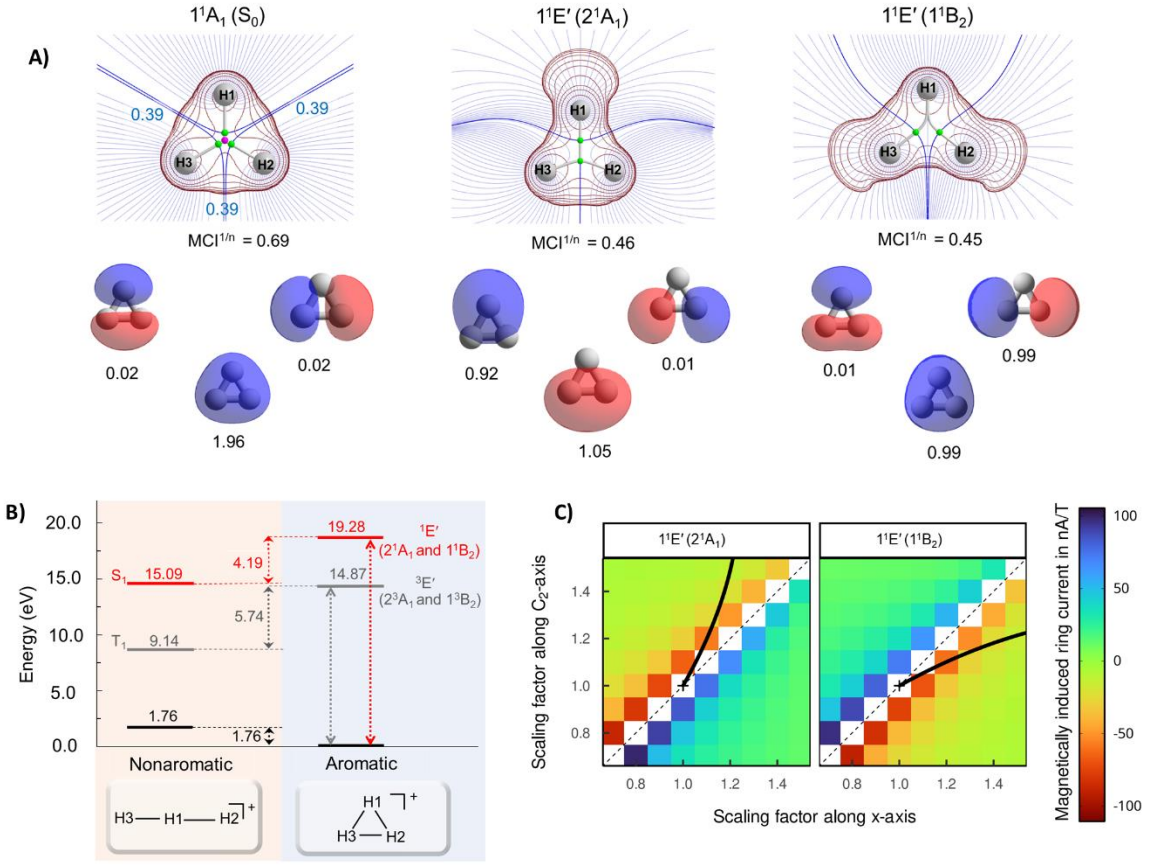

Figure 3. **Ground state aromaticity and excited state antiaromaticity of H_3^+**: (A) Topological analysis of the electron density, 2D Laplacian of the electron density (in red), and natural orbitals (with populations) for the S_0 and $1^1E'$ states, the latter labelled as 2^1A_1 and 1^1B_2 in C_{2v} symmetry. The rays of the basins are shown in blue, and density gradient lines are shown in purple. The MCI$^{1/n}$ values (computed using Becke-rho's partition)(*37*) given below the Laplacian plots of the electron density. (B) Vertical excitation energies and relative energies of H_3^+ at, respectively, $D_{\infty h}$ and D_{3h} symmetries. (C) Magnetically induced ring currents calculated for the 2^1A_1 and 1^1B_2 states which stem from the $1^1E'$ states upon geometric distortions to C_{2v} symmetric structures. The scaling factors reflect how large this distortion was (a value of 1 represents the H–H bond lengths of the S_0 equilibrium geometry). The C_2-axis indicates distortions in the direction of forming an acute isosceles triangle (moving H1 atom) and the *x*-axis

indicates distortions along an obtuse isosceles triangle formation (increasing the separation between H2 and H3).

With regard to the electron densities of these states and their Laplacians, they exhibit significant differences from those of S_0, which corroborates the loss of aromaticity upon excitation (Figure 3A). Despite the D_{3h} symmetric geometry of H_3^+ in its vertically excited states, the electron density distribution has lower symmetry as it shifts toward the outer part of the atoms, preceding the dissociations that occur upon excitation to these states. Although the H atoms are still covalently bonded, as indicated by the value of the DIs, the 2^1A_1 and 1^1B_2 states exhibit drastic reductions of the three-center delocalization to 37 - 39% of the MCI value of S_0 (Figure 3A). Similar conclusions can be reached on the antiaromaticity of the $1^3E'$ (1^3A_1 and 1^3B_2) states based on the analysis of the electron delocalization in Figure S2.(*35*) Thus, the $MCI^{1/n}$ values for H_3^+ (0.62 (S_0), 0.46 and 0.45 ($1^1E'$), and 0.39 and 0.36 ($1^3E'$)), are comparable to those of benzene in its S_0, S_1, and T_1 states (0.59, 0.40, and 0.36, respectively).(*36*) This is consistent with an aromatic S_0 and antiaromatic lowest excited singlet and triplet states ($1^1E'$ and $1^3E'$).

At the S_0 state equilibrium geometry, the values of the magnetically induced ring current obtained for the vertically excited $1^1E'$ states diverge as a result of the two-fold degeneracy at D_{3h} symmetry. The analysis of ring current strength at the C_{2v} symmetric structures reveals that the $1^1E'$ states exhibit a pole in the ring current at D_{3h} symmetric geometries (Figure 3C), *i.e.*, a sudden change from highly diatropic to highly paratropic values, which explains the divergence observed at the vertical excitation. This resembles recent observations on the transient antiaromatic states of the *c*-C_{16} molecule where small bond length alterations lead to changes from dia- to paratropicity, or *vice versa*,(*38*) related to the orbital degeneracies at highly symmetric structures.(*39*) Now, by following the C_{2v} symmetric dissociation paths of

H_3^+, and thus, the 2^1A_1 and 1^1B_2 states, we observe gradually diminishing paratropic ring currents (Figure 3C), in line with antiaromaticity relief. Also the $NICS(0)_{zz}$ values computed along these paths reveal antiaromaticity, with values of 77.1 and 84.7 ppm at two C_{2v} symmetric structures distorted by a factor 1.5, leading to, respectively, acute and obtuse isosceles triangular structures as exemplified in Figure 2B (see further SI Section S3).

Protons-to-electrons ratios and impacts

Having established the antiaromaticity of the $1^1E'$ states of H_3^+, the question is if the GSA-to-ESAA switch in character (Figure 1B) explains the unusually high vertical excitation energy of this cation. From computations of light atoms, molecules and ions with only two electrons such as He, Li^+, HeH^+ and He_2^{2+} (Table S3), we see that high vertical excitation energies are characteristic of these species, which mostly cannot exhibit aromaticity as they are acyclic. Many of these ions are also found in space, *e.g.*, Li^+ and HeH^+.(*40*) Indeed, it has been argued that HeH^+ was the first molecule of the Universe,(*41-43*) and it produces H_2^+ upon collision with atomic H, which in turn can produce H_3^+ in a reaction with H_2.

The excitation energies are higher for more positively charged species, and is highest when the protons are concentrated in one nucleus (He, Li^+ and Be^{2+}). Hence, in the 3p,2e series, Li^+ and HeH^+ feature higher vertical $E(S_1)$ than H_3^+ by, respectively, 41.16 and 6.91 eV, and similar for the vertical $E(T_1)$ (Table S3). For the 2e species He, Li^+ and Be^{2+}, with protons-to-electrons ratios of 1.0, 1.5 and 2.0, respectively, the first excitation energy goes up dramatically from 20.94 eV to 60.44 eV and 121.26 eV as the excitation implies a gradually larger loss in the electrostatic attraction between electrons and nuclei.

Now, to estimate the impact of the protons-to-electrons ratio on the excitation energies, we explored the π-conjugated and S_0 aromatic cyclopropenium cation, *c*-$C_3H_3^+$, which has an equilateral triangular structure and a near-unit ratio of 1.05 between total nuclear and electronic

charges (+21 *vs.* -20) (SI sections S5 and S6).(*44-46*) Indeed, *c*-$C_3H_3^+$ is isolobal with H_3^+, *i.e.*, its π-orbitals are analogous to the σ-orbitals of H_3^+.(*47*) Thus, it helps us decipher the relative contributions of the protons-to-electrons ratio *versus* the GSA-to-ESAA switch to the 19.28 eV excitation energy of H_3^+.

The vertical transition to the lowest ππ* states ($1^1E''$) of *c*-$C_3H_3^+$ requires 9.71 eV. This is only half that of the transition to the σσ* states of H_3^+ but significantly higher than the lowest ππ* states of any other π-bonded hydrocarbon, *e.g.*, 7.11 eV for ethylene.(*48*) Thus, *c*-$C_3H_3^+$ has its lowest ππ* states at an unusually high excitation energy despite its near-unit protons-to-electrons ratio. Therefore, the high excitation energy of the lowest ππ* transition of *c*-$C_3H_3^+$ is not caused by a drastically diminished electrostatic attraction upon excitation. Instead, it should arise from the stabilization in the S_0 state due to aromaticity plus destabilization in the ππ* states due to antiaromaticity, and this applies also to the lowest triplet states. From this one can estimate that the additional energy (9.57 eV) to reach the excitation energy of H_3^+ is caused by the electrostatic effect.

Comparisons to analogous carbocations

Further analysis of the *c*-$C_3H_3^+$ cation, which also is of astrochemical importance,(*49*) enables us to show that the very high first excitation energy of H_3^+ is due to both stabilization by GSA plus destabilization by ESAA and the high protons-to-electrons ratio. The isomerization stabilization energy (ISE)(*50*) of *c*-$C_3H_3^+$ in S_0, computed as the reaction energy for the 1,3-hydrogen shift from a nonaromatic isomer to the S_0 aromatic methylcyclopropenium cation (Figure 4A), is -2.03 eV with CCSD. This reveals a stronger aromatic character than that of benzene in S_0 (-1.34 eV with CCSD/aug-cc-pVDZ). In contrast, the lowest vertically excited singlet and triplet ππ* states exhibit large positive ISE values of 2.66 and 2.78 eV with EOM-CCSD,

corresponding to strong excited state antiaromatic destabilization. Accordingly, the S_0 stabilization plus excited state antiaromatic destabilizations of *c*-$C_3H_3^+$ are 4.69 and 4.81 eV, respectively, and these should represent lower bounds for the analogous energies in H_3^+.

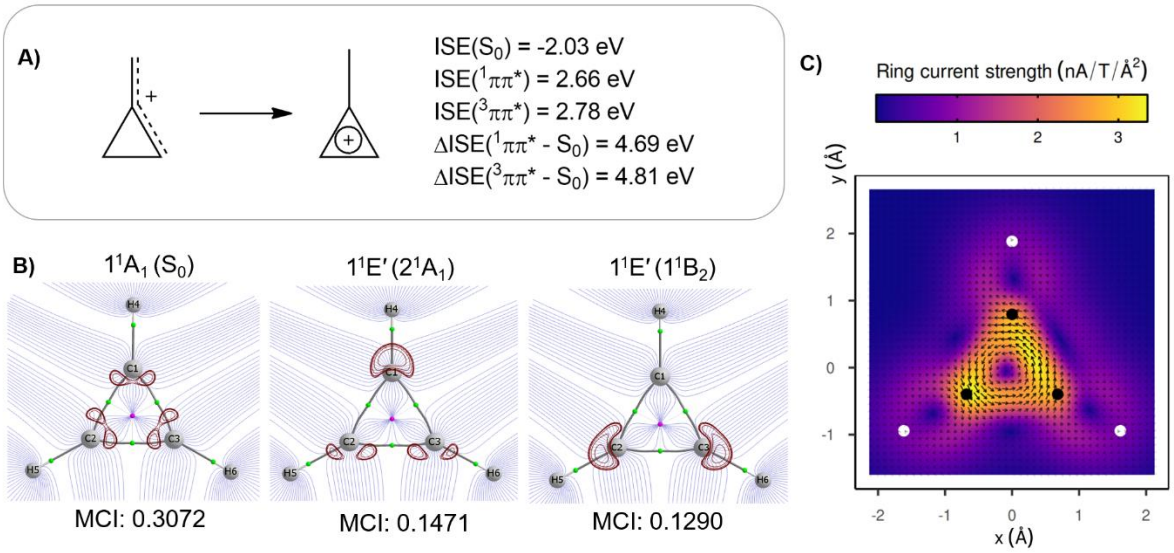

Figure 4. **Ground state aromaticity and excited state antiaromaticity of *c*-$C_3H_3^+$**: (A) Isomerization stabilization energies (ISEs) of the methylcyclopropenium cation in the S_0 and lowest vertically excited singlet and triplet ππ* states, and the combined ISEs. (B) Topological analysis and Laplacian of the electron density (in red) of S_0 and excited states of *c*-$C_3H_3^+$ at its S_0 geometry (1.0 a.u. above ring plane) and MCI values. (C) MICD of the cyclopropenium cation in its $1^1E''$ (1^1B_2) state vertically excited from S_0 showing paratropic (antiaromatic) ring currents (1.0 a.u. above ring plane). Carbon atoms plotted as black balls and hydrogen atoms as white.

A comparison of the linear H_3^+ with the allyl cation ($H_2CCHCH_2^+$) allows for a second assessment of the impact of the high protons-to-electrons ratio of H_3^+. The two species are isolobal and nonaromatic in S_0, yet have different protons-to-electrons counts (3:2 *vs*. 23:22). For the allyl cation, with a near-unit protons-to-electrons ratio, the lowest vertical ππ* singlet

state is found at 5.50 eV, while the first σσ* excitation energy of linear H_3^+ is 13.33 eV, *i.e.*, 7.83 eV higher than that of the allyl cation. Both this and the excitation energy difference between *c*-$C_3H_3^+$ and H_3^+ (9.57 eV) provide estimates of the electrostatic contribution to excitation energies of H_3^+ species.

Antiaromaticity assessments of *c*-$C_3H_3^+$ in its first singlet excited ππ* state reveal a clear resemblance to H_3^+. The MCI values demonstrate their electronic structural similarities with the values for, respectively, the $1^1E'$ and $1^1E''$ states being less than half those of the S_0 state (Figures 3 and 4B), and this is further emphasized by the topological analysis of their excited state electronic structures (Figures 3A and 4B). Finally, the MICD of the cyclopropenium cation in its lowest ππ* state reveals a paratropic (antiaromatic) ring current in the three-membered ring (Figure 4C), similar as for the two dissociation pathways of H_3^+ (Figure 3C).

Thus, *c*-$C_3H_3^+$ like H_3^+, exhibit strong aromaticity in the S_0 state and strong antiaromaticity in the lowest electronically excited states, yet the excitation energy of the latter is additionally affected by a high protons-to-electrons ratio. Indeed, by adding energy additives to the lowest excitation energy of the acyclic and nonaromatic allyl cation (5.50 eV) one can estimate the excitation energy of H_3^+. The energy for the GSA-to-ESAA switch in character in *c*-$C_3H_3^+$ (4.69 eV) and the excitation energy difference between the allyl cation and linear H_3^+ or between triangular *c*-$C_3H_3^+$ and H_3^+ (7.83 – 9.57 eV), as measures of the electrostatic energy loss between protons and electrons upon excitation, added to 5.50 eV gives 18.0 – 19.8 eV. This energy range brackets our computed first excitation energy of H_3^+ of 19.28 eV.

Conclusions

We decipher the energy contributors to the very high electronic excitation energy of H_3^+, which enables its astrochemical and astrophysical functions, through a comparison of triangular H_3^+ with linear H_3^+ and two analogous π-conjugated hydrocarbon ions, the cyclopropenium cation

(*c*-$C_3H_3^+$) and allyl cation ($CH_2CHCH_2^+$). Had the vertical excitation energy been lower, H_3^+ would have been more prone to photodissociate in space. We reveal that three factors are important; (*i*) the change from a stabilizing aromatic character to (*ii*) a destabilizing antiaromatic character upon excitation from S_0 to the lowest excited states (present also in *c*-$C_3H_3^+$), and (*iii*) the high ratio between total nuclear and electronic charges (present also in small cations). These three factors together provide the origin of the astrophotochemical inertness of H_3^+. Without this photostability H_3^+ could not have had the functions it has in the Universe. Indeed, it would have led to a different Universe from the one we know.

We show for the first time that excited state antiaromaticity is a molecular electronic structure property with crucial astrochemical influence that also has astrophysical implications. In a broader sense, our findings point to the roles of excited state aromaticity and antiaromaticity as important new concepts for interpretation in astrochemistry. We anticipate that these effects impact on a number of photochemical processes in space.

Supplementary information

Section S1: Computational details; Section S2: Energies and geometries of H_3^+; Section S3: Aromaticity of H_3^+, electronic properties; Section S4: Aromaticity of H_3^+, magnetic properties; Section S5: Protons-to-electrons ratios; Section S6: Cyclopropenium cation ($C_3H_3^+$); Section S7: Supplementary references.

Author contributions

Conceptualization: HO; Supervision: HO; Project Administration: HO; Funding Acquisition: HO; Methodology: HO, CFN, EM; Analysis: JMT and JS; Investigation: JMT and JS; Visualization: JMT and JS; Writing – Original Draft: JMT; Writing – Review & Editing: JMT, JS, EM, CFN, HO.

Acknowledgements

First of all, H.O. is grateful to his neighbor, Prof. em. Bengt Gustafsson, for getting him on the path towards astrochemistry. All authors thank Dr. Radovan Bast for extensive help with the magnetically induced current density calculations, Mr. Hannes Gustafsson and Dr. Lucia Corti for involvement in preliminary calculations, and Prof. Jochen Autschbach, Prof. Paul Barklem, Prof. Eszter Borbas, Dr. Stefano Crespi, Dr. Gaurab Ganguly, Dr. Victor Gray, Prof. Martin Rahm, Prof. Andrew Teale, Prof. Yann Trolez, Prof. Philippe Wernet and Prof. Judy Wu for discussions on the project at various stages. The computations were enabled by resources provided by the National Academic Infrastructure for Supercomputing in Sweden (NAISS) and the Swedish National Infrastructure for Computing (SNIC) at the National Supercomputer Center (NSC), Linköping, Sweden, through grant agreements 2022/5-378, 2023/5-335 and 2024/5-422. The Foundation Olle Engkvist Byggmästare is greatly acknowledged for a post-doctoral fellowship to J. M. T. (grant 184-390). H.O. thanks the Swedish Research Council for financial support (grants 2019-05618 and 2023-04179). E.M. is grateful for the funding and technical support provided by the Donostia International Physics Center (DIPC), and grant PID2022-140666NB-C21 funded by MCIN/AEI/10.13039/501100011033 and "FEDER Una manera de hacer Europa". C.F.-N. thanks National Science Centre, Poland 2020/39/B/ST4/02022 for funding.

References

1. T. Oka, Interstellar H_3^+. *Chem. Rev.* **113**, 8738-8761 (2013).
2. T. R. Geballe, T. Oka, Detection of H_3^+ in interstellar space. *Nature* **384**, 334-335 (1996).
3. M. Larsson, H_3^+: the initiator of interstellar chemistry. *Int. J. Astrobiol.* **7**, 237-241 (2008).

4. S. Miller, T. Stallard, H. Melin, J. Tennyson, H_3^+ cooling in planetary atmospheres. *Faraday Discuss.* **147**, 283-291 (2010).

5. G. Kannan, J. R. Chien, A. J. Benjamin, N. Bhatia, R. J. Saykally, Rydberg states of H_3 and HeH as potential coolants for primordial star formation. *J. Phys. Chem. A* **125**, 4267-4275 (2021).

6. R. W. A. Havenith, F. De Proft, P. W. Fowler, P. Geerlings, σ-aromaticity in $H_3^+$and Li_3^+: Insights from ring-current maps. *Chem. Phys. Lett.* **407**, 391-396 (2005).

7. S. Sadjadi, On the topology of the electron density of H_3^+. *Struct. Chem.* **28**, 1445-1452 (2017).

8. C. Foroutan-Nejad, P. Rashidi-Ranjbar, Chemical bonding in the lightest tri-atomic clusters; H_3^+, Li_3^+ and B_3^-. *J. Mol. Struct. THEOCHEM* **901**, 243-248 (2009).

9. D. Zhao *et al.*, in *Atomic Clusters with Unusual Structure, Bonding and Reactivity*, P. K. Chattaraj, S. Pan, G. Merino, Eds. (Elsevier, 2023), pp. 237-245.

10. M. Solà, A. I. Boldyrev, M. K. Cyrański, T. M. Krygowski, G. Merino, *Aromaticity and antiaromaticity: Concepts and applications*. (John Wiley & Sons, Ltd, 2023).

11. M. Pavanello, L. Adamowicz, High-accuracy calculations of the ground, 1 $^1A_1'$, and the 2 $^1A_1'$, 2 $^3A_1'$, and 1 $^1E'$ excited states of H_3^+. *J. Chem. Phys.* **130**, 034104 (2009).

12. A. Petrignani *et al.*, Ultraviolet and visible light photodissociation of H_3^+ in an ion storage ring. *J. Phys. Chem. A* **114**, 4864-4869 (2010).

13. X. Urbain, A. Dochain, R. Marion, T. Launoy, J. Loreau, Photodissociation as a probe of the H_3^+ avoided crossing seam. *Phil. Trans. R. Soc. A* **377**, 20180399 (2019).

14. K. Kawaoka, R. F. Borkman, Single-center calculations on the electronically excited states of equilateral H_3^+ ion. *J. Chem. Phys.* **54**, 4234-4238 (1971).

15. E. v. Dishoeck, H. R. Hrodmarsson, Leiden photodissociation and photoionization cross section database. **2024**, (**2023**);

https://home.strw.leidenuniv.nl/~ewine/photo/display_h3+_f8a0eca1bcc94c898fc68220d4b45be8.html).

16. H. R. Hrodmarsson, E. F. van Dishoeck, Photodissociation and photoionization of molecules of astronomical interest. *A&A* **675**, (2023).

17. A. N. Heays, A. D. Bosman, E. F. van Dishoeck, Photodissociation and photoionisation of atoms and molecules of astrophysical interest. *A&A* **602**, (2017).

18. S. Lepp, P. C. Stancil, A. Dalgarno, Atomic and molecular processes in the early Universe. *J. Phys. B: At., Mol. Opt. Phys.* **35**, R57 (2002).

19. E. F. van Dishoeck, Photodissociation processes of astrophysical molecules. *Symp. - Int. Astron. Union* **120**, 51-65 (1987).

20. D. Galli, F. Palla, The dawn of chemistry. *Annu. Rev. Astron. Astrophys.* **51**, 163-206 (2013).

21. L. Adamowicz, M. Pavanello, Progress in calculating the potential energy surface of H_3^+. *Phil. Trans. R. Soc. A* **370**, 5001-5013 (2012).

22. A. V. Turbiner, J. C. Lopez Vieyra, Ground state of the H_3^+ molecular ion: physics behind. *J. Phys. Chem. A* **117**, 10119-10128 (2013).

23. J. Tennyson, O. L. Polyansky, N. F. Zobov, A. Alijah, A. G. Császár, High-accuracy calculations of the rotation-vibration spectrum of H_3^+. *J. Phys. B: At., Mol. Opt. Phys.* **50**, 232001 (2017).

24. N. C. Baird, Quantum organic photochemistry. II. Resonance and aromaticity in the lowest $^3\pi\pi^*$ state of cyclic hydrocarbons. *J. Am. Chem. Soc.* **94**, 4941-4948 (1972).

25. M. Rosenberg, C. Dahlstrand, K. Kilså, H. Ottosson, Excited state aromaticity and antiaromaticity: opportunities for photophysical and photochemical rationalizations. *Chem. Rev.* **114**, 5379-5425 (2014).

26. R. Papadakis, H. Ottosson, The excited state antiaromatic benzene ring: a molecular Mr Hyde? *Chem. Soc. Rev.* **44**, 6472-6493 (2015).

27. J. Kim, J. Oh, A. Osuka, D. Kim, Porphyrinoids, a unique platform for exploring excited-state aromaticity. *Chem. Soc. Rev.* **51**, 268-292 (2022).

28. J. Yan, T. Slanina, J. Bergman, H. Ottosson, Photochemistry driven by excited-state aromaticity gain or antiaromaticity relief. *Chem. Eur. J.* **29**, e202203748 (2023).

29. F. Feixas, E. Matito, J. Poater, M. Solà, Quantifying aromaticity with electron delocalisation measures. *Chem. Soc. Rev.* **44**, 6434-6451 (2015).

30. R. F. W. Bader, M. E. Stephens, Fluctuation and correlation of electrons in molecular systems. *Chem. Phys. Lett.* **26**, 445-449 (1974).

31. R. F. W. Bader, M. E. Stephens, Spatial localization of the electronic pair and number distributions in molecules. *J. Am. Chem. Soc.* **97**, 7391-7399 (1975).

32. P. Bultinck, R. Ponec, S. Van Damme, Multicenter bond indices as a new measure of aromaticity in polycyclic aromatic hydrocarbons. *J. Phys. Org. Chem.* **18**, 706-718 (2005).

33. Y. Mo, P. v. R. Schleyer, An energetic measure of aromaticity and antiaromaticity based on the Pauling–Wheland resonance energies. *Chem. Eur. J.* **12**, 2009-2020 (2006).

34. X. Lin, Y. Mo, On the bonding nature in the crystalline tri-thorium cluster: Core-shell syngenetic σ-aromaticity. *Angew. Chem. Int. Ed. Engl.* **61**, e202209658 (2022).

35. E. Matito, An electronic aromaticity index for large rings. *Phys. Chem. Chem. Phys.* **18**, 11839-11846 (2016).

36. F. Feixas, J. Vandenbussche, P. Bultinck, E. Matito, M. Solà, Electron delocalization and aromaticity in low-lying excited states of archetypal organic compounds. *Phys. Chem. Chem. Phys.* **13**, 20690-20703 (2011).

37. E. Matito, M. Solà, P. Salvador, M. Duran, Electron sharing indexes at the correlated level. Application to aromaticity calculations. *Faraday Discuss.* **135**, 325-345 (2007).

38. I. Rončević *et al.*, Aromaticity reversal induced by vibrations in cyclo[16]carbon. *J. Am. Chem. Soc.* **145**, 26962-26972 (2023).

39. E. Steiner, P. W. Fowler, Patterns of ring currents in conjugated molecules: A few-electron model based on orbital contributions. *J. Phys. Chem. A* **105**, 9553-9562 (2001).

40. L. González-Sánchez, N. Sathyamurthy, F. A. Gianturco, The role of small molecular cations in the chemical flow of the interstellar environments. *Phys. Chem. Chem. Phys.* **25**, 23370-23383 (2023).

41. R. C. Fortenberry, The oldest molecular ancestor finally brought into the light. *Chem* **5**, 1028-1030 (2019).

42. Y. Mi *et al.*, D_3^+ formation through photoionization of the molecular D_2–D_2 dimer. *Nat. Chem.* **15**, 1224-1228 (2023).

43. R. Güsten *et al.*, Astrophysical detection of the helium hydride ion HeH^+. *Nature* **568**, 357-359 (2019).

44. R. Breslow, J. T. Groves, G. Ryan, Cyclopropenyl cation. *J. Am. Chem. Soc.* **89**, 5048-5048 (1967).

45. M. N. Glukhovtsev, S. Laiter, A. Pross, Thermochemical assessment of the aromatic and antiaromatic characters of the cyclopropenyl cation, cyclopropenyl anion, and cyclopropenyl radical: A high-level computational study. *J. Phys. Chem.* **100**, 17801-17806 (1996).

46. K. B. Wiberg, P. R. Rablen, Re-examination of some carbocations. Structures, energies, and charge distributions. *J. Org. Chem.* **85**, 11741-11749 (2020).

47. R. Hoffmann, Building bridges between inorganic and organic chemistry (Nobel lecture). *Angew. Chem. Int. Ed.* **21**, 711-724 (1982).

48. R. S. Mulliken, The excited states of ethylene. *J. Chem. Phys.* **66**, 2448-2451 (1977).

49. A. Ali, E. C. Sittler, D. Chornay, B. R. Rowe, C. Puzzarini, Cyclopropenyl cation – the simplest Huckel's aromatic molecule – and its cyclic methyl derivatives in Titan's upper atmosphere. *Planet Space Sci.* **87**, 96-105 (2013).

50. P. v. R. Schleyer, F. Pühlhofer, Recommendations for the evaluation of aromatic stabilization energies. *Org. Lett.* **4**, 2873-2876 (2002).